Identification of the strain-dependent coefficient of permeability by combining the results of experimental and numerical oedometer tests with free lateral movement

Anis Balic[a], Emina Hadzalic[*] and Samir Dolarevic[b]

Faculty of Civil Engineering, University of Sarajevo, Patriotske lige 30, 71000 Sarajevo, Bosnia and Herzegovina

Abstract. The key parameter that affects the consolidation process of soil is the coefficient of permeability. The common assumption in the consolidation analysis is that the coefficient of permeability is porosity-dependent. However, various authors suggest that the strain-dependency of the coefficient of permeability should also be taken into account. In this paper, we present results of experimental and numerical analyses, with an aim to determine the strain-dependency of the coefficient of permeability. We present in detail both the experimental procedure and the finite element formulation of the two-dimensional axisymmetric numerical model of the oedometer test (standard and modified). We perform a set of experimental standard and modified oedometer tests. We use these experimental results to validate our numerical model and to define the model input parameter. Finally, by combining the experimental and numerical results, we propose the expression for the strain-dependent coefficient of permeability.

Keywords: Biot's theory; consolidation; free lateral movement; numerical model; oedometer test; permeability; strain-dependency

1. Introduction

The consolidation represents the time change in the volume of the saturated soil due to applied load. Namely, when the load is applied to the saturated soil, it is first carried by the water in the pores, which causes the rapid increase in the pore water pressures, called excess pore pressures. The excess pore pressure build-up causes the water to drain out of the pores. During this process, the load is gradually transferred from pore water to the soil skeleton, resulting in the rise of the effective stresses. This causes the compression of the soil skeleton, resulting in a decrease in the soil volume, i.e., the settlements. After the excess pore pressures drop to zero, there is no more change in the effective stresses, hence neither in the volume of the soil sample, and we can state that the consolidation has ended. One of the key parameters that determine the rate of soil consolidation is the permeability of the soil, expressed through the coefficient of permeability (Liang *et al.* 2017). For high-permeability soils, such as sand or gravel, the consolidation occurs

---

*Corresponding author, Assistant Professor, E-mail: emina.hadzalic@gf.unsa.ba
[a]Assistant Professor, E-mail: anis.balic@gf.unsa.ba
[b]Professor, E-mail: samir.dolarevic@gf.unsa.ba

practically immediately after the load is applied. On the other hand, for low-permeability soils, such as clays, the consolidation can last for a very long time, measured in years.

The pioneering works in the mathematical formulation of soil consolidation are Terzaghi's theory of one-dimensional consolidation (Terzaghi 1943) and Biot's theory of three-dimensional consolidation (Biot 1941). Both theories assume that the soil is linear elastic, deformations are small, and the pore water flow is governed by Darcy's law. Furthermore, the compressibility and the permeability of the soil are assumed constant during the consolidation process.

Biot's theory of three-dimensional consolidation is commonly used in the numerical modeling of the solid phase-pore fluid interaction problems (Singh and Sawant 2014, Tasiopoulou *et al.* 2015a, 2015b, Hadzalic *et al.* 2018, 2019, 2020, Radhika *et al.* 2020), such as the embankment consolidation analysis (Borges 2004, Huang *et al.* 2006, Al-Shakarchi *et al.* 2009, Oliveira nad Lemos 2011). The end result of the embankment consolidation analysis is the consolidation curve: time-embankment settlement, which is used in the embankment design and the embankment construction schedule. The value of the embankment settlement is controlled by the deformability parameters of the soil, and the rate of the settlement by the coefficient of permeability, which is usually assumed to be to be porosity-dependent (Di and Sato 2003, Xie and Leo 2004, Zhuang *et al.* 2005, Geng *et al.* 2006, Zou *et al.* 2017, Plaxis 3D Reference Manual 2021). The coefficient of permeability of the soil can be determined directly from the constant head or falling head permeability tests, or indirectly from the standard oedometer test.

In a standard oedometer test, the lateral movements of the soil sample are restrained and the deformation occurs only in the vertical direction. The load is applied, and the settlements of the soil sample in time are monitored. The conditions simulated in the standard oedometer test are valid only in narrow central areas in the soil under the embankment, where the lateral movements are indeed prevented (Fig. 1, zone A) (Wood 2009). However, in other areas, this assumption no longer holds since the deformation occurs in both vertical and horizontal directions (Fig. 1, zone B and C). Due to this, various authors suggest that the strain-dependency of the coefficient of permeability should also be taken into account in the numerical analysis of soil consolidation (Rowe 1959, Kirby and Blunden 1991, Wong and Li 2001).
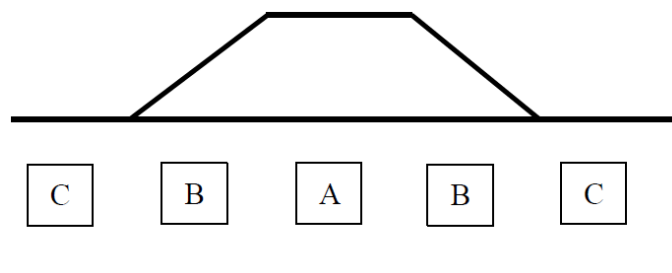
Fig. 1 Zones in soil under the embankment with different strain states

In this paper, we aim to establish the relation between the strain state and the coefficient of permeability. To achieve this goal, we combine the results of experimental and numerical analyses. First, we confirm the strain-dependency through a series of experimental tests on clay samples. Namely, we measure the value of the coefficient of permeability before and after sample deformation in a modified oedometer test, which allows lateral movements. For determining the

value of the coefficient of permeability we use the falling head permeability test. Next, we form a numerical model of the oedometer test. First, we verify the proposed numerical model by comparing the computed results for a standard oedometer test against those obtained experimentally. Second, we combine the experimental results with the results of numerical simulations of the modified oedometer test, and we propose the expression for the strain-dependent coefficient of permeability.

The outline of the paper is as follows. In Section 2, we introduce an experimental testing procedure for confirming the strain-dependency of the coefficient of permeability, which combines the falling head permeability test and modified oedometer test. In Section 3, we present the main details of the finite element formulation of a two-dimensional axisymmetric numerical model of the standard and the modified oedometer test. In Section 4, we present the results of experimental and numerical analyses. We compare the computed results against those obtained experimentally, and we propose the expression for the strain-dependent coefficient of permeability. In Section 5, we give our concluding remarks.

2. Experimental analysis

The coefficient of permeability k can be determined directly from the constant head or falling head permeability tests, or indirectly from the coefficient of consolidation c_v, which is commonly determined from the standard oedometer test. The relation between the coefficient of permeability and the coefficient of consolidation is given as

$$c_v = \frac{k \cdot E_{oed}}{\gamma_w} \tag{1}$$

where E_{oed} is the oedometer or constrained modulus, and γ_w is the unit weight of the water. The relation between the oedometer modulus, and Young's modulus E and Poisson ratio ν is given as

$$E_{oed} = E \frac{(1-\nu)}{(1+\nu)(1-2\nu)} \tag{2}$$

In this Section, we first aim to experimentally confirm the strain-dependency of the coefficient of permeability. To do so, we combine the falling head permeability test and the modified oedometer test. Namely, we first conduct a falling head permeability test on a clay sample and obtain the value of the coefficient of permeability before deformation. Next, we subject the clay sample to deformation by performing a modified oedometer test, which allows lateral movement. Finally, we repeat the falling head permeability test on a deformed clay sample, and we obtain the value of the coefficient of permeability after deformation. In total, we test five clay samples from two different locations (Table 1).

The falling permeability test is performed in a specially designed apparatus (Fig. 2), which enables the test to be conducted before and after the deformation of the sample. Namely, the device is equipped with two profiled pipes with diameters of 94 mm and 79 mm. We first perform the falling head permeability test for the clay sample 20 mm high with a diameter of 94 mm placed in the larger diameter pipe. Next, we cut the sample to the diameter of 70 mm required by the apparatus for the oedometer test, and we perform the modified oedometer test. Finally, we again perform the falling head permeability test where we place the deformed sample from the modified

1- soil sample
2- porous plate
3- profiled pipe
   a- profiled pipe for testing before
      modified oedometer test
   b- profiled pipe for testing after
      modified oedometer test
4- threaded rod
5- ring
6- box
7- standpipe
8- water
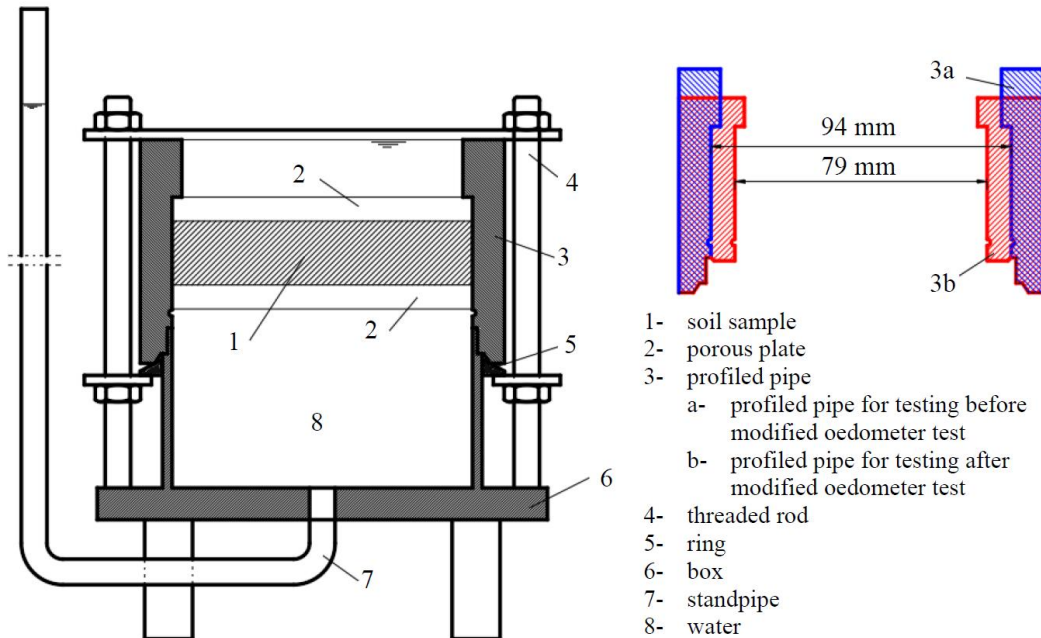
Fig. 2 Modified falling head permeability test

1- soil sample
2- porous plate
3- stiff ring
4- top cap
5- external box
6- water
7- dial gauge
8- load
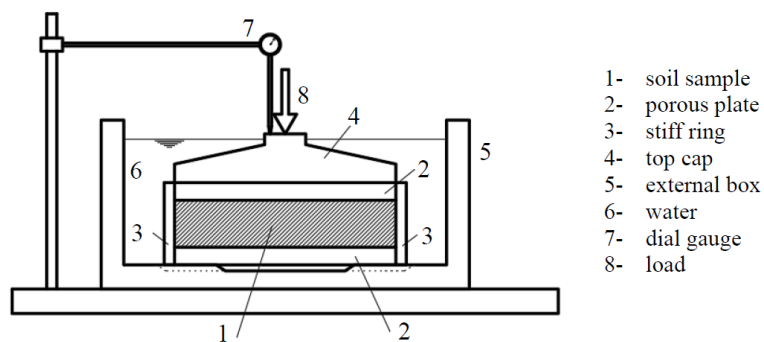
Fig. 3 Standard oedometer test

oedometer test in the pipe with a diameter of 79 mm. The profile pipe diameter of 79 mm is chosen because the diameter of the deformed sample from the modified oedometer test is no longer 70 mm, but larger due to free lateral movement. The new diameter of the sample is known only after the test. Due to this, we have chosen the diameter of 79 mm, to be able to use the same profiled pipe for all tested samples. The gap between the pipe and the sample has been sealed with acrylic putty in order to ensure the flow of the water only through the clay sample.

The modified oedometer test is conducted by removing the stiff ring which prevents lateral movement from the standard odometer apparatus (Fig. 3). The modified oedometer test is performed as follows: A clay sample 20 mm high with a diameter of 70 mm, placed between the porous plates, is submerged into the water and loaded with the vertical load of 100 kPa. The settlement of the sample in time is monitored. The testing ends when the consolidation curve time-settlement flattens out, suggesting the end of the consolidation.

Table 1 Experimentally obtained values of coefficient of permeability before and after deformation

Sample No.	Location	Coefficient of permeability before deformation k_A [10^{-9} cm/s]	Coefficient of permeability after deformation k_B [10^{-9} cm/s]	Ratio
1	Bugojno	2.82	8.51	3.02
2	Bugojno	2.53	7.43	2.94
3	Bugojno	2.85	9.43	3.34
4	Maglaj	6.70	13.7	2.05
5	Maglaj	10.2	24.5	2.40

Table 2 Experimental results of standard oedometer tests

Sample No.	Location	Coefficient of consolidation c_v [10^{-4} cm^2/s]	Initial settlement s_p [mm]	Settlement during primary consolidation s_{pk} [mm]	Oedometer moduli E_{oed} [kPa]
a	Bugojno	3.70	0,106	0.0840	23 683
b	Bugojno	4.03	0,344	0.1060	18 543
c	Bugojno	3.67	0,418	0.1035	18 919
d	Maglaj	4.02	0,423	0.0555	36 732

The experimentally obtained values of the coefficient of permeability before and after the deformation are presented in Table 1. The experimental results confirm that the coefficient of permeability depends on the strain state of the sample.

We also perform standard oedometer tests with an aim to use the results from these tests to validate our numerical model for the case of the standard oedometer test. In total, we test four clay samples from two different locations (Table 2). The results of experimental tests in terms of coefficient of consolidation, initial settlement, settlement during primary consolidation, and oedometer moduli are summarized in Table 2. The initial settlement is due to adjustment of the sample and the porous plates, and its value can be significantly larger than the settlement during the primary consolidation. This initial settlement is not included in the numerical model, which is presented in the next Section.

3. Numerical model

In this Section, we present a two-dimensional axisymmetric numerical model of the oedometer test (standard and modified), which implements Biot's theory of consolidation (Lewis and Schrefler 1998, Smith and Griffiths 2004, Zienkiewicz and Taylor 2005, Ibrahimbegovic 2009).

The basic assumptions of Biot's theory are that the soil is saturated and linear elastic, the deformations are small, the pore water and soil particles are incompressible, and the pore water flow is governed by Darcy's law. Biot's theory assumes that the compressibility and the permeability of the soil remain constant during the consolidation process.

To define the governing equations of the coupled problem, Biot's theory combines equilibrium and continuity equation. The equilibrium equation implements Terzhagi's principle of effective stresses, which states that the total normal stress σ is equal to the sum of the effective stress σ' carried by the soil skeleton and the pore pressure p carried by the water in the pores, written as

$$\sigma = \sigma' + bp \tag{3}$$

where b is the Biot coefficient; if the soil particles and the water in the pores are assumed to be incompressible, which are basic assumptions in soil mechanics, then $b=1$. The effective part of the total normal stress is computed from the constitutive equations.

The strong form of the equilibrium equation in cylindrical coordinates is written as

$$
\begin{aligned}
\frac{\partial \sigma_r}{\partial r} + \frac{\sigma_r - \sigma_\theta}{r} + \frac{\partial \tau_{zr}}{\partial z} &= 0 \\
\frac{\partial \tau_{rz}}{\partial r} + \frac{\tau_{rz}}{r} + \frac{\partial \sigma_z}{\partial z} &= 0
\end{aligned}
\tag{4}
$$

where σ_r is the radial normal stress, σ_θ is the tangential normal stress, σ_z is the vertical normal stress, τ_{rz} is the shear stress, r is the distance from the axis of symmetry, and z is the vertical coordinate axis.

The constitutive equations for the linear elastic behavior of soil are written as

$$
\begin{aligned}
\sigma'_r &= (2\mu + \lambda)\varepsilon_r + \lambda\varepsilon_z + \lambda\varepsilon_\theta \\
\sigma'_z &= \lambda\varepsilon_r + (2\mu + \lambda)\varepsilon_z + \lambda\varepsilon_\theta \\
\tau_{rz} &= \mu\gamma_{rz} \\
\sigma'_\theta &= \lambda\varepsilon_r + \lambda\varepsilon_\theta + (2\mu + \lambda)\varepsilon_\theta
\end{aligned}
\tag{5}
$$

where ε_r is the radial strain, ε_θ is the tangential strain, ε_z is the vertical strain, γ_{rz} is the shear strain, and λ and μ are Lame's coefficients. The strains are given as

$$
\varepsilon_r = \frac{\partial u}{\partial r}; \qquad \varepsilon_z = \frac{\partial w}{\partial z}; \qquad \varepsilon_\theta = \frac{2\pi(r+u) - 2\pi r}{2\pi r} = \frac{u}{r}; \qquad \gamma_{rz} = \frac{\partial u}{\partial z} + \frac{\partial w}{\partial r}
\tag{6}
$$

where u and w are displacements in the radial and vertical direction.

The strong form of the continuity equation is written as

$$
\frac{\partial}{\partial t}\left(\frac{\partial u}{\partial r} + \frac{\partial w}{\partial z}\right) - \frac{k_r}{\gamma_w}\frac{1}{r}\frac{\partial p}{\partial r} - \frac{k_r}{\gamma_w}\frac{\partial^2 p}{\partial r^2} - \frac{k_z}{\gamma_w}\frac{\partial^2 p}{\partial z^2} = 0
\tag{7}
$$

where k_r and k_z are the coefficients of permeability in the radial and vertical direction, p is the pore pressure, and γ_w is the unit weight of the water.

Next, we perform the standard finite element discretization procedure and we introduce the finite element approximations for the unknown displacement and pore pressure fields. For finite element approximation of displacement and pore pressure fields, we use **Q8**-**P4** finite element, which assumes quadratic interpolation of the displacement field and linear interpolation of the pore pressure field.

The end result of the standard finite element discretization procedure is the following global system of equations, written as

$$
\begin{aligned}
\mathbf{K}_m\mathbf{u} + \mathbf{C}\mathbf{p} &= \mathbf{f} \\
\mathbf{C}^{\mathrm{T}}\dot{\mathbf{u}} - \mathbf{K}_c\mathbf{p} &= \mathbf{0}
\end{aligned}
\tag{8}
$$

where $\mathbf{K}_m$ is the stiffness matrix, $\mathbf{K}_c$ is the permeability matrix, $\mathbf{C}$ is the coupling matrix, $\mathbf{f}$ is the

external load vector, $\mathbf{u}$ is the vector of unknown nodal displacements, $\dot{\mathbf{u}}$ is the vector of time derivatives of nodal displacements, and $\mathbf{p}$ is the vector of unknown nodal pore pressures.

For the standard oedometer test, where lateral movements are restrained and the strain ε_θ is equal to zero, the stiffness matrix $\mathbf{K}_m$, the permeability matrix $\mathbf{K}_c$, the coupling matrix $\mathbf{C}$ are written as

$$\mathbf{K}_m = \iint \mathbf{B}^{\mathrm{T}} \mathbf{D} \mathbf{B} r dr dz; \quad \mathbf{K}_c = \iint \mathbf{T}^{\mathrm{T}} \mathbf{k} \mathbf{T} r dr dz; \quad \mathbf{C} = \iint \mathbf{M} \mathbf{N}^P r dr dz \tag{9}$$

where

$$\mathbf{D} = \begin{bmatrix} \lambda + 2\mu & \lambda & 0 & \lambda \\ \lambda & \lambda + 2\mu & 0 & \lambda \\ 0 & 0 & \mu & 0 \\ \lambda & \lambda & 0 & \lambda + 2\mu \end{bmatrix}; \mathbf{k} = \begin{bmatrix} \dfrac{k_r}{\gamma_w} & 0 \\ 0 & \dfrac{k_z}{\gamma_w} \end{bmatrix};$$

$$\mathbf{M} = \begin{bmatrix} \dfrac{\partial N_1^u}{\partial r} & \dfrac{\partial N_1^u}{\partial z} & \cdots & \dfrac{\partial N_i^u}{\partial r} & \dfrac{\partial N_i^u}{\partial z} & \cdots & \dfrac{\partial N_8^u}{\partial r} & \dfrac{\partial N_8^u}{\partial z} \end{bmatrix};$$

$$\mathbf{N}^P = \begin{bmatrix} N_1^p & N_2^p & N_3^p & N_4^p \end{bmatrix};$$

$$\mathbf{B} = \begin{bmatrix} \dfrac{\partial N_1^u}{\partial r} & 0 & \cdots & \dfrac{\partial N_i^u}{\partial r} & 0 & \cdots & \dfrac{\partial N_8^u}{\partial r} & 0 \\ 0 & \dfrac{\partial N_1^u}{\partial z} & \cdots & 0 & \dfrac{\partial N_i^u}{\partial z} & \cdots & 0 & \dfrac{\partial N_8^u}{\partial z} \\ \dfrac{\partial N_1^u}{\partial z} & \dfrac{\partial N_1^u}{\partial r} & \cdots & \dfrac{\partial N_i^u}{\partial z} & \dfrac{\partial N_i^u}{\partial r} & \cdots & \dfrac{\partial N_8^u}{\partial z} & \dfrac{\partial N_8^u}{\partial r} \\ \dfrac{N_1^u}{r} & 0 & \cdots & \dfrac{N_i^u}{r} & 0 & \cdots & \dfrac{N_8^u}{r} & 0 \end{bmatrix}; \mathbf{T}^{\mathrm{T}} = \begin{bmatrix} \dfrac{\partial N_1^p}{\partial r} & \dfrac{\partial N_1^p}{\partial z} \\ \dfrac{\partial N_2^p}{\partial r} & \dfrac{\partial N_2^p}{\partial z} \\ \dfrac{\partial N_3^p}{\partial r} & \dfrac{\partial N_3^p}{\partial z} \\ \dfrac{\partial N_4^p}{\partial r} & \dfrac{\partial N_4^p}{\partial z} \end{bmatrix} \tag{10}$$

Here, N^u denotes the quadratic interpolation function for the displacement field, and N^p denotes the linear interpolation function for the pore pressure field.

For the modified oedometer test, where lateral movements are not restrained and the ε_θ is not equal to zero, in some members of the matrices, r appears in the denominator, which prevents the value of these members to be computed accurately when r approaches zero (Smith and Griffiths 2004). To solve this problem, both equations in (8) are multiplied with r, which results in modified $\mathbf{B}$ and $\mathbf{T}$ matrices that contains the derivatives of shape functions and modified external load vector $\mathbf{f}$. The stiffness matrix $\mathbf{K}_m$, the permeability matrix $\mathbf{K}_c$, the coupling matrix $\mathbf{C}$, for the modified oedometer test, are written as

$$\mathbf{K}_m^* = \iint \mathbf{B}^{\mathrm{T},*} \mathbf{D} \mathbf{B}^* dr dz; \quad \mathbf{K}_c^* = \iint \mathbf{T}^{\mathrm{T},*} \mathbf{k} \mathbf{T}^* dr dz; \quad \mathbf{C}^* = \iint \mathbf{M}^* \mathbf{N}^P r dr dz \tag{11}$$

where

$$\mathbf{M}^* = \begin{bmatrix} \dfrac{\partial N_1^u}{\partial r} r & \dfrac{\partial N_1^u}{\partial z} r & \cdots & \dfrac{\partial N_i^u}{\partial r} r & \dfrac{\partial N_i^u}{\partial z} r & \cdots & \dfrac{\partial N_8^u}{\partial r} r & \dfrac{\partial N_8^u}{\partial z} r \end{bmatrix};$$

$$
\mathbf{B}^* = \begin{bmatrix} \dfrac{\partial N_1^u}{\partial r}r & 0 & \cdots & \dfrac{\partial N_i^u}{\partial r}r & 0 & \cdots & \dfrac{\partial N_8^u}{\partial r}r & 0 \\[2mm] 0 & \dfrac{\partial N_1^u}{\partial z}r & \cdots & 0 & \dfrac{\partial N_i^u}{\partial z}r & \cdots & 0 & \dfrac{\partial N_8^u}{\partial z}r \\[2mm] \dfrac{\partial N_1^u}{\partial z}r & \dfrac{\partial N_1^u}{\partial r}r & \cdots & \dfrac{\partial N_i^u}{\partial z}r & \dfrac{\partial N_i^u}{\partial r}r & \cdots & \dfrac{\partial N_8^u}{\partial z}r & \dfrac{\partial N_8^u}{\partial r}r \\[2mm] N_1^u & 0 & \cdots & N_i^u & 0 & \cdots & N_8^u & 0 \end{bmatrix} ; \ \mathbf{T}^* = \begin{bmatrix} \dfrac{\partial N_1^p}{\partial r}r & \dfrac{\partial N_1^p}{\partial z}r \\[2mm] \dfrac{\partial N_2^p}{\partial r}r & \dfrac{\partial N_2^p}{\partial z}r \\[2mm] \dfrac{\partial N_3^p}{\partial r}r & \dfrac{\partial N_3^p}{\partial z}r \\[2mm] \dfrac{\partial N_4^p}{\partial r}r & \dfrac{\partial N_4^p}{\partial z}r \end{bmatrix} \quad (12)
$$

The global system of equations is solved by the means of the trapezoidal rule (Smith and Griffiths 2004).

4. Numerical results

In this Section, we present the results of several numerical simulations. First, we validate our numerical model of the standard oedometer test by comparing computed results in terms of consolidation curves against those obtained experimentally. Next, by combining experimental and numerical results of the modified oedometer test, we propose the expression for the strain-dependent coefficient of permeability.

All numerical implementations and simulations are performed by using the finite element code developed by the authors in Fortran. The geometry of the model, finite element mesh, and the boundary conditions for standard and modified oedometer test are shown in Fig. 4. The dimensions of the clay sample are 20×33 mm. The stone porous plate, 3 mm thick, is placed on the top of the sample. The sample is loaded with 100 kPa.
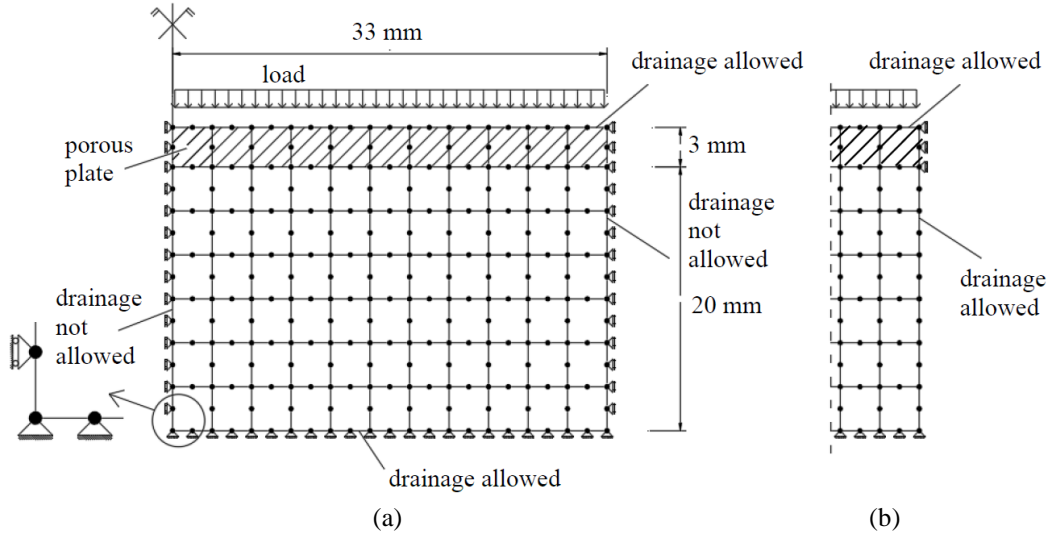
Fig. 4 Geometry of the model, boundary conditions and finite element mesh (a) standard oedometer test (b) modified oedometer test

We assume that the stone porous plate and the clay sample are linear elastic. The material properties of the stone porous plate are: Young's modulus E=30 000 MPa, Poisson's ratio v=0.2, and coefficient of permeability k=10 000 mm/min.

In all numerical simulations, we assume that the coefficient of permeability and oedometer moduli of clay sample change in time but that the coefficient of consolidation remains constant (Eq. (1)) (Davis and Raymond 1965). For both numerical models of standard and oedometer tests, we explain in detail how the values of these parameters are selected.

4.1 Standard oedometer test

In Table 3, we give the average values of coefficient of permeability by locations: the average values of coefficient of permeability before and after deformation, and the values of coefficient of permeability computed from average values of coefficient of consolidation and oedometer moduli, obtained from standard oedometer tests, using Eq. (1).

Table 3 Average values of coefficient of permeability by locations

Sample No.	Location	Coefficient of permeability before deformation k_A [10^{-9} cm/s]	Coefficient of permeability after deformation k_B [10^{-9} cm/s]	Coefficient of permeability obtained from Eq. (1) k_C [10^{-9} cm/s]
I	Bugojno	2.73	8.46	1.94
II	Maglaj	8.45	19.1	1.11

From the results shown in Table 3, we can conclude that the average values of coefficient of permeability before deformation k_A obtained from the falling head test are about 40% higher than the values of coefficient of permeability obtained using Eq. (1). The difference is due to the initial settlement in the standard oedometer test, which is due to the porous plates adjustment. In order to overcome this difference, the initial value of the coefficient of permeability k_0 in our numerical model is obtained by combining the values k_A and k_C using the following expression

$$k_0 = k_A - \frac{s_p}{s_p + s_{pk}} \left(k_A - k_C \right) \tag{13}$$

The coefficient of permeability is assumed to be porosity-dependent. The porosity dependence coefficient of permeability is usually defined with the following expression (Plaxis 3D Reference Manual 2021)

$$k = k_0 \cdot 10^{\frac{e_0 - e}{c_k}} \tag{14}$$

where e_0 is the initial void ratio of the clay sample, e is the void ratio of clay sample in time and c_k is the constant (0.4-0.5) e_0.

In our numerical simulations, we assume that the coefficient of permeability changes from the initial value computed based on the initial void ratio, and the final value computed based on the final value of the void ratio. The initial void ratio e_0 and the final void ratio e_k are obtained from the experimental standard oedometer tests for different locations. Based on the initial value of the coefficient of permeability and initial oedometer moduli, we can compute the coefficient of

Table 4 Input material parameters of clay sample for numerical model of standard oedometer test

Sample No.	I	II
Location	Bugojno	Maglaj
Initial void ratio e_0	0.690	0.568
Final void ratio e_k	0.681	0.564
Initial coefficient of permeability k_0 [10^{-9} cm/s]	2.13	1.96
Final coefficient of permeability k_k [10^{-9} cm/s]	1.98	1.88
Initial oedoemeter moduli $E_{oed,0}$ [kPa]	18 649	35 273
Final oedoemeter moduli $E_{oed,k}$ [kPa]	20 103	36 732
Coefficient of consolidation [10^{-4} cm^2/s]	4.05	7.05
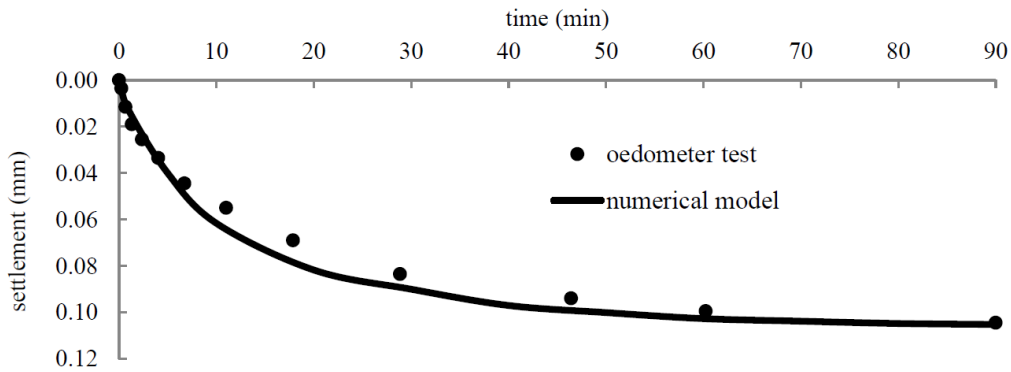
Fig. 5 Numerical and experimental consolidation curves for standard oedometer test, location Bugojno
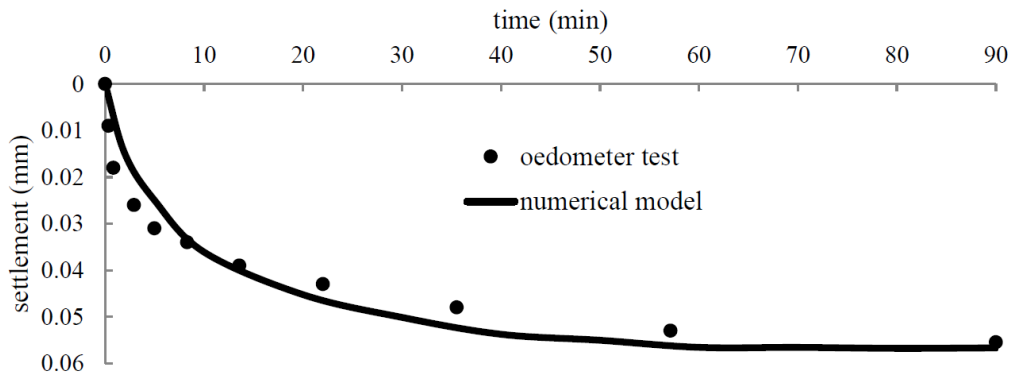
Fig. 6 Numerical and experimental consolidation curves for standard oedometer test, location Maglaj

consolidation of the clay sample, which we assume remains constant throughout the simulation. Using Eq. (1) we are able to compute the final value of the coefficient of permeability k_k. Then, from the known value of the coefficient of consolidation and the final value of the coefficient of permeability, we are able to compute the final value of oedometer moduli. The input material parameters of the clay sample for the numerical model of the standard oedometer test are given in Table 4.

In our numerical simulations, the values of the coefficient of permeability and oedometer moduli are linearly increased at each time step from the initial to the final value, whereas the value

of the coefficient of the consolidation remains constant at each time step.

The results of numerical simulations in terms of consolidation curves are given in Figs. 4 and 5. We can conclude that the computed consolidation curves show a good match with those obtained experimentally.

Next, we perform the numerical simulations of the modified oedometer test in order to establish the strain-dependency of the coefficient of permeability.

4.2 Modified oedometer test

The oedometer modulus is the modulus that corresponds to the conditions of restrained lateral movement. The values of initial oedometer modulus given in Table 4 are obtained from an experimentally performed standard oedometer test, in which the lateral movements of the sample are restrained. If these values were to be used in numerical simulations of the modified oedometer test, we would not be able to obtain a match between numerical and experimental results, because of different boundary conditions. Thus, the new initial and the final value of oedometer moduli are obtained by matching the experimentally and numerically obtained values of settlement, for the case of the modified oedometer test. On the basis of the assumption that the coefficient of consolidation remains constant with the values given in Table 4, the initial and the final value of the coefficient of permeability are computed using Eq. (1). The input material parameters of the clay sample for the numerical model of the modified oedometer test are given in Table 5.

In our numerical simulations, the values of the coefficient of permeability and oedometer moduli are linearly increased at each time step from the initial to the final value, whereas the value of the coefficient of the consolidation remains constant at each time step. The experimental and

Table 5 Input material parameters of clay sample for numerical model of modified oedometer test

Sample No.	I	II
Location	Bugojno	Maglaj
Initial coefficient of permeability k_0 [10^{-9} cm/s]	2.66	2.10
Final coefficient of permeability k_k [10^{-9} cm/s]	3.39	2.63
Initial oedoemeter moduli $E_{oed,0}$ [kPa]	14 906	32 958
Final oedoemeter moduli $E_{oed,k}$ [kPa]	11 731	26 330
Coefficient of consolidation [10^{-4} cm^2/s]	4.05	7.05
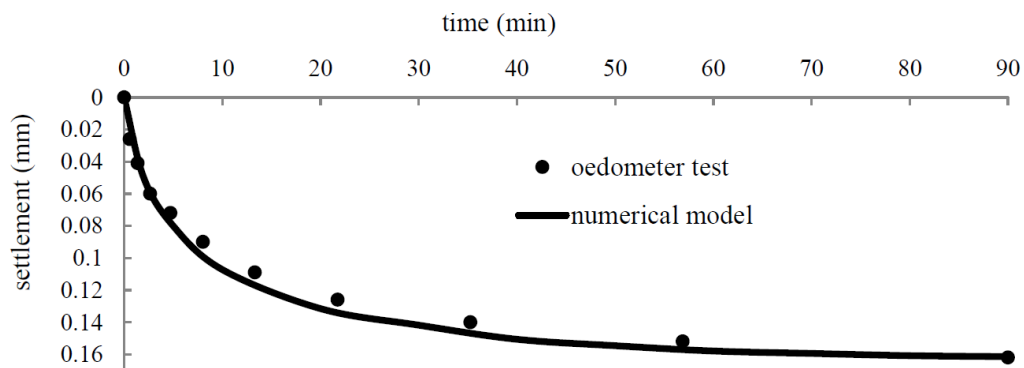
Fig. 7 Numerical and experimental consolidation curves for modified oedometer test, location Bugojno
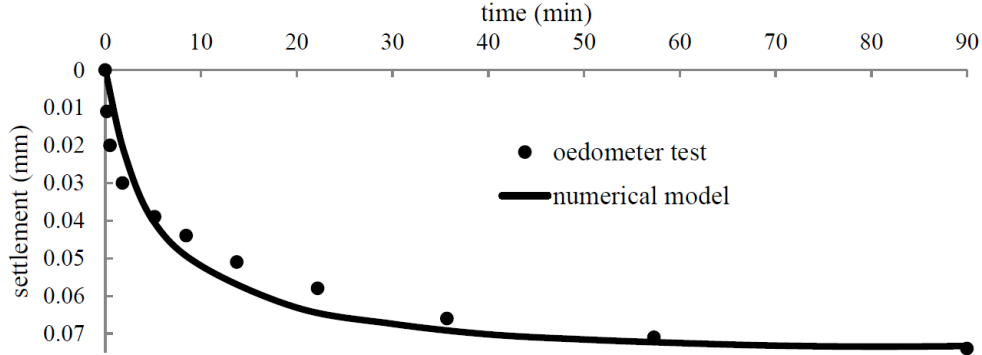
Fig. 8 Numerical and experimental consolidation curves for standard oedometer test, location Maglaj

computed consolidation curves are shown in Figs. 6 and 7. We can conclude that a good match between the results is obtained.

Next, we aim to identify the strain-dependency of the coefficient of permeability. We assume that the strain-dependency of the coefficient of permeability is defined with the following expression

$$k = \alpha \cdot \frac{\varepsilon_s / \varepsilon_v}{0.66} \cdot k_0 \cdot 10^{\frac{e_0 - e}{c_k}} \tag{15}$$

where ε_v is the volumetric deformation, ε_s is the shear deformation, α is the coefficient of the change in permeability, and the value of 0.66 represents the ratio of shear and volumetric deformation in standard oedometer test. The volumetric deformation ε_v and the shear deformation ε_s, are computed as

$$\begin{Bmatrix} \delta \varepsilon_v \\ \delta \varepsilon_s \end{Bmatrix} = \begin{bmatrix} 1 & 2 \\ \dfrac{2}{3} & -\dfrac{2}{3} \end{bmatrix} \begin{Bmatrix} \delta \varepsilon_z \\ \delta \varepsilon_r \end{Bmatrix} \tag{16}$$

The change in the void ratio Δe at each time step is computed following the expression

$$\Delta e = \Delta \varepsilon_v \cdot (1 + e_0) \tag{17}$$

where $\Delta \varepsilon_v$ is the change in the volumetric deformation. At each time step, the new value of void ratio e is equal to

$$e = e_0 - \Delta e \tag{18}$$

Then, based on the computed value of the void ratio, and computed values of volumetric and shear deformation, we proceed to compute the numerical value of the coefficient of permeability using Eq. (15). The only unknown parameter in Eq. (15) is the parameter α. We identify this parameter by matching the expression on the right side of Eq. (15) with the input value of the coefficient of permeability. The identified values of parameter α for locations Bugojno and Maglaj are given in Table 6.

Table 6 Identified values of the coefficient of the change in permeability α

Sample No.	I	II
Location	Bugojno	Maglaj
Coefficient of change in permeability α [-]	0.355	0.329

5. Conclusions

In this paper, we have performed experimental and numerical oedometer tests, both standard and modified, with an aim to identify the strain-dependency of the coefficient of permeability.

First, we have presented an experimental testing procedure, which combines the falling head permeability test and oedometer test. The obtained experimental results confirm the assumption that the value of the coefficient of permeability depends on the strain state. Next, we have presented a two-dimensional axisymmetric numerical model of the oedometer test, which implements Biot's porous media theory. The input values of model parameters are obtained from experimental results. The numerical model was first validated by comparing the computed consolidation curves against those obtained experimentally, for the case of the standard oedometer test. Then, by performing the numerical simulations of the modified oedometer test and by combining the experimental and numerical results, the expression for strain-dependency of the coefficient of permeability is proposed, and the unknown parameter of change in permeability α is identified.

The research in this paper can have practical importance, Namely, the use of the strain-dependent value of the coefficient of permeability in the embankment design can result in the earlier start of works on pavement structure, hence in an earlier finish of the complete works. The plans for future works include an extension to the case of nonlinear behavior of soil.

References

Al-Shakarchi, Y.J., Fattah, M.Y. and Al-Shammary, A.S.J. (2009), "Finite element analysis of embankments on soft clays-Case studies", *J. Eng.*, **15**(1),3268-3292.

Biot, M.A. (1941), "General theory of three-dimensional consolidation", *J. Appl. Phys.*, **1941**(12), 155-164. https://doi.org/10.1063/1.1712886.

Borges, J.L. (2004), "Three-dimensional analysis of embankments on soft soils incorporating vertical drains by finite element method", *Comput. Geotech.*, **31**(8), 665-676. https://doi.org/10.1016/j.compgeo.2004.11.001.

Davis, E.H. and Raymond, G.P. (1965), "A non-linear theory of consolidation", *Geotechnique*, **15**(2), 161-173. https://doi.org/10.1680/geot.1965.15.2.161.

Di, Y. and Sato, T. (2003), "Liquefaction analysis of saturated soils taking into account variation in porosity and permeability with large deformation", *Comput. Geotech.*, **30**(7), 623-635. https://doi.org/10.1016/S0266-352X(03)00060-0.

Geng, X., Xu, C. and Cai, Y. (2006), "Non-linear consolidation analysis of soil with variable compressibility and permeability under cyclic loadings", *Int. J. Numer. Anal. Meth. Geomech.*, **30**, 803-821. https://doi.org/10.1002/nag.505.

Hadzalic, E., Ibrahimbegovic, A. and Dolarevic, S. (2019), "Theoretical formulation and seamless discrete approximation for localized failure of saturated poro-plastic structure interacting with reservoir", *Comput. Struct.*, **214**, 73-93. https://doi.org/10.1016/j.compstruc.2019.01.003.

Hadzalic, E., Ibrahimbegovic, A. and Dolarevic, S. (2020), "3D thermo-hydro-mechanical coupled discrete beam lattice model of saturated poro-plastic medium", *Couple. Syst. Mech.*, **9**(2), 125-145. http://doi.org/10.12989/csm.2020.9.2.125.

Hadzalic, E., Ibrahimbegovic, A. and Nikolic, M. (2018), "Failure mechanisms in coupled poroplastic medium", *Couple. Syst. Mech.*, **7**(1), 43-59. http://doi.org/10.12989/csm.2018.7.1.043.

Huang, W., Fityus, S., Bishop, D., Smith, D. and Sheng, D. (2006), "Finite-element parametric study of the consolidation behavior of a trial embankment on soft clay", *Int. J. Geomech.*, **6**(5), 328-341. https://doi.org/10.1061/(ASCE)1532-3641(2006)6:5(328).

Ibrahimbegovic, A. (2009), *Nonlinear Solid Mechanics: Theoretical Formulations and Finite Element Solution Methods*, Springer.

Kirby, J.M. and Blunden, B.G. (1991), "Interaction of soil deformations, structure and permeability", *Soil Res.*, **29**, 891-904. https://doi.org/10.1071/SR9910891.

Lewis, R.W. and Schrefler, B.A. (1998), *The Finite Element Method in the Static and Dynamic Deformation and Consolidation of Porous Media*, John Wiley and Sons.

Liang, F., Song, Z. and Jia, Y. (2017), "Hydro-mechanical behaviors of the threedimensional consolidation of multi-layered soils with compressible constituents", *Ocean Eng.*, **131**, 272-282. https://doi.org/10.1016/j.oceaneng.2017.01.009.

Oliveira, P.J.V. and Lemos, L.J.L. (2011), "Numerical analysis of an embankment on soft soils considering large displacement", *Comput. Geotech.*, **38**(1), 88-93. https://doi.org/10.1016/j.compgeo.2010.08.005.

Plaxis 3D Reference Manual (2021), Bentley.

Radhika, B.P., Krishnamoorthy, A. and Rao, A.U. (2020), "A review on consolidation theories and its application", *Int. J. Geotech. Eng.*, **14**(1), 9-15. https://doi.org/10.1080/19386362.2017.1390899.

Rowe, P.W. (1959), "Measurement of the coefficient of consolidation of lacustrine clay", *Geotechnique*, **9**(3), 107-118. https://doi.org/10.1680/geot.1959.9.3.107.

Singh, M. and Sawant, V.A. (2014), "Parametric study on flexible footing resting on partially saturated soil", *Couple. Syst. Mech.*, **3**(2), 233-245. http://doi.org/10.12989/csm.2014.3.2.233.

Smith, M. and Griffiths, D.V. (2004), *Programming the Finite Element Method*, 4th Edition, John Wiley & Sons.

Tasiopoulou, P., Taiebat, M., Tafazzoli, N. and Jeremic, B. (2015a), "Solution verification procedures for modeling and simulation of fully coupled porous media: Static and dynamic behavior", *Couple. Syst. Mech.*, **4**(1), 67-98. http://doi.org/10.12989/csm.2015.4.1.067.

Tasiopoulou, P., Taiebat, M., Tafazzoli, N. and Jeremic, B. (2015b), "On validation of fully coupled behavior of porous media using centrifuge test results", *Couple. Syst. Mech.*, **4**(1), 37-65. http://doi.org/10.12989/csm.2014.4.1.037.

Terzaghi, K. (1943), *Theoretical Soil Mechanics*, Wiley.

Wong, R.C.K. and Li, Y. (2001), "A deformation-dependent model for permeability changes in oil sand due to shear dilation", *J. Can. Petrol. Technol.*, **40**(08), PETSOC-01-08-03. https://doi.org/10.2118/01-08-03.

Wood, D.M. (2009), *Soil Mechanics: A One-Dimensional Introduction*, Cambridge University Press, New York.

Xie, K.H. and Leo, C.J. (2009), "Analytical solutions of one-dimensional large strain consolidation of saturated and homogeneous clays", *Comput. Geotech.*, **31**(4), 301-314. https://doi.org/10.1016/j.compgeo.2004.02.006.

Zhuang, Y.C., Xie, K.H. and Li, X.B. (2005), "Nonlinear analysis of consolidation with variable compressibility and permeability", *J. Zhejiang Univ. Sci.*, **6A**(3), 181-187. https://doi.org/10.1007/BF02872317.

Zienkiewicz, O.C. and Taylor, R.L. (2005), *The Finite Element Method*, Vols. I, II, III, Elsevier.

Zou, S.F., Li, J.Z., Wang, Z.J., Lan, L., Wang, W.J. and Xie, X.Y. (2017), "Seepage test and empirical models for soils based on GDS apparatus", *J. Zhejiang Univ. Sci. (Eng. Sci.)*, **51**(5), 856-862.